38th International Electric Vehicle Symposium and Exhibition (EVS38) Göteborg, Sweden, June 15-18, 2025

Electrochemical performance attenuation of silicon/graphite-based lithium-ion batteries under intermittent overcharge cyclic aging conditions

Gang Wei, Ranjun Huang, Jixiang Cai, Bo Jiang, Haifeng Dai*
School of Automotive Studies, Tongji University, No. 4800, Caoan Road, Shanghai 201804, China
tongjidai@tongji.edu.cn

Executive Summary

Lithium-ion batteries exhibit a high probability of intermittent overcharge cycle accumulation during long-term operation due to the cross-cell inconsistencies and the potential failures in the battery management system. However, the impact of such condition on the electrochemical performance attenuation of batteries remains insufficiently explored. In this study, the battery cyclic aging tests under two types of intermittent overcharge conditions with different overcharge degrees and one normal condition are carried out, and comparison of dominant aging mechanisms during battery cyclic aging by electrochemical impedance spectroscopy and incremental capacity-differential voltage non-destructive analysis methods. The results show that when the upper cut-off voltage increases (4.4 V), the accelerating capacity decay and impedance growth occur; after further increasing to a certain degree (4.6 V), it can cause the nonlinear decay of capacity and exponential growth of impedance, which is closely related to the more severe loss of active material and loss of lithium inventory.

Keywords: Electric Vehicles; Batteries; Battery Management System; Energy Storage Systems; Life Cycle Analysis

1 Introduction

Lithium-ion batteries (LIBs) are widely used in the development of electric vehicles (EVs) and the construction of new energy storage systems (ESSs) due to their high energy density and long cycle life [1]. However, due to the need for large-scale grouping, battery inconsistency and malfunction of the battery management system (BMS) may cause the battery's operating range to exceed the predetermined value, i.e., electrical abuse. One of the typical forms of electrical abuse is overcharge, which may lead to performance attenuation and even safety failure [2].

Battery failure severity varies depending on the overcharge degree, and it is extremely serious cases that can lead to battery fire or even explosion. Mao et al. [3] and Zhang et al. [4] systematically investigated the effect of overcharge rate value on the thermal runaway characteristics of $Li(Ni_{0.6}Mn_{0.2}Co_{0.2})O_2$ (NMC622)/graphite and LFP/graphite batteries, respectively, and the results show that only the rate value exceeds a certain degree can induce a rapid temperature rise. When the overcharge rate value is certain, the overcharge cut-off voltage is an important factor affecting the battery failure degree. As mentioned above, if the upper cut-off voltage is not limited, there is a high probability that thermal runaway will be triggered. Considering the control function of the BMS, it is more consistent with practical application scenarios to explore the battery failure behavior after it is overcharged to a certain upper cut-off voltage. In order to

investigate the attenuation effect of a single severe overcharge on the battery performance, Zhang et al. [5] carried out the single overcharge test with an upper cut-off voltage of up to 5.0 V for $Li(Ni_{0.8}Mn_{0.1}Co_{0.1})O_2$ (NMC811)/graphite batteries, and the results showed that the capacity decrease is minor, but still larger compared to the capacity attenuation caused by a charge in the normal voltage range. Moreover, Zhang et al. [6] conducted the cyclic aging test for $Li(Ni_xCo_yAl_zO_2)$ (NCA)/graphite batteries with an overcharge cut-off voltage of up to 5.0 V. The results showed that the discharge capacity attenuation exceeds 10 % of the initial capacity after only 15 cycles. In summary, severe overcharge abuse will cause battery safety accidents and abnormally accelerated lifetime degradation. In addition to the above failure scenarios being overly serious in terms of the overcharge degree, the continuous overcharge behavior may not be consistent with the practical operating characteristics. There have been many studies on battery performance attenuation due to continuous overcharge [7,8], but there is still a lack of studies involving intermittent overcharge. It is obvious that intermittent overcharge is a type of operating condition that needs to be fully investigated to reveal the failure mechanism of battery performance attenuation under this type of operating condition.

To address the above gaps, two intermittent overcharge cyclic aging conditions with different overcharge degrees and one normal cyclic aging condition are set up in this study to investigate the battery performance attenuation characteristics and corresponding failure mechanisms under such operating conditions by using non-destructive analysis methods. Meanwhile, it can be found that the existing studies are mostly carried out for graphite anode-based batteries, which are less involved in the case of new high energy density anodes. Therefore, considering that the improvement of anode energy density is also an essential aspect in the industrial pursuit of superior battery performance, the silicon/graphite composite anode-based battery, which represents one of the trends for future applications, is chosen as the study object.

2 Experiments

2.1 Battery samples and formation tests

The tested battery sample (Fig. 1(a)) in this study is the customized pouch-type lithium-ion battery, with a nominal capacity of 1.0 Ah. The cell's dimensions are 63 mm in length, 50 mm in width, and 3 mm in thickness. The cathode is NCM811, and the anode is artificial graphite + 5 wt.% SiO_x. The separator is a PE film with ceramic coating. Since cycling aging tests need to be carried out in this study, to eliminate possible calendar aging factors involved, all tested pouch batteries are non-electrolyte-containing cells, which are purchased directly from Li-FUN New Energy Technology Company Ltd., Zhuzhou, Hunan Province, China. The recommended electrolyte amount is 4.5 g/pc. The type of electrolyte used is 1M $LiPF_6$ in EC: EMC=3:7 vol%, which is purchased from Suzhou DuoDuo Chemical Technology Company. The equipment used for electrolyte injection is a vacuum injection machine (MSK-113-PVM, Fig. 1(b)). Prior to the formation procedure, the cell is rested for 24 h after filling with the appropriate amount of electrolyte to allow the electrolyte to fully wet the electrodes.

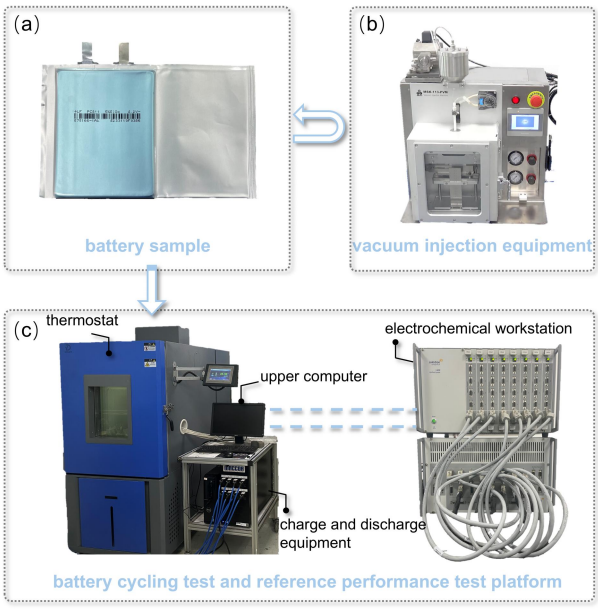

Figure 1: (a) battery sample; (b) vacuum injection equipment; (c) battery cycling test and reference performance

test platform.

The voltage characteristics during the formation process, capacity calibration after formation and electrochemical impedance spectroscopy (EIS) at different states of charge (SoCs) after formation are shown in Fig. 2. The formation protocol consists of 3 cycles between 3.0 and 4.2 V. The formation process is performed through charging with 0.05 C to 4.2 V and then discharging with 0.05 C to 3.0 V. The rest time between the charging and discharging processes is 1 h. After the formation process is completed, the battery capacity is calibrated using standard charging and discharging profiles, i.e., charging to 4.2 V with 0.5 C, then charging at constant voltage (CV) until the current is less than 0.05 C, and finally discharging to 3.0 V with 0.2 C, and this is repeated for 3 cycles. The rest time between the charging and discharging processes is 30 min. The results show that the standard discharge capacity of the fabricated battery is about 1.02 Ah, and the coulombic efficiency of the charge/discharge cycle is about 99.8%; in addition, the EIS characteristics of the battery at 100%, 50% and 0% SoC exhibit normal electrochemical performance. The above indicates that the battery obtained by this method can be further used for cyclic aging tests.

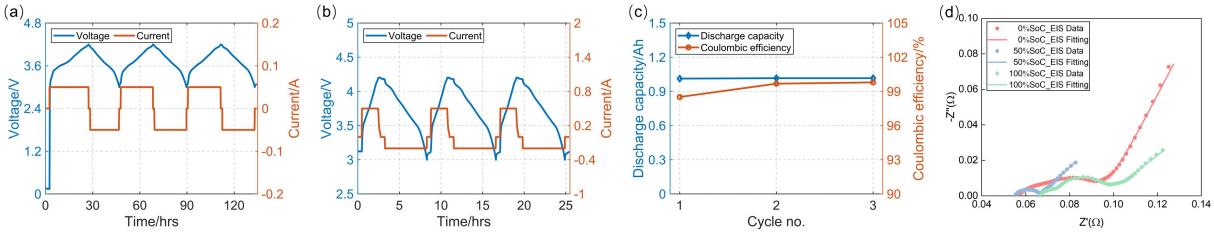

Figure 2: (a) battery voltage and current during formation; (b) standard discharge capacity calibration after formation; (c) discharge capacity values and coulombic efficiency values during capacity calibration process; (d) impedance characteristics at different SoCs after formation.

2.2 Battery cyclic aging tests

The battery cycling test platform (Fig. 1(c)) includes the upper computer, the battery charge/discharge equipment (Maccor 4000), and the thermostat (DONG & YE). The ambient temperature during cycling is controlled at room temperature of 25°C. Considering the randomness and unpredictability of overcharge behavior in practical scenarios, this study chooses a medium overcharge frequency of 0.5 as the basic feature for constructing the intermittent overcharge cyclic aging conditions, i.e., the occurrence ratio between the overcharge cyclic condition and the normal cyclic condition is 1:1, to systematically explore the impact of intermittent overcharge behavior on battery performance attenuation. In addition, two types of overcharge upper cut-off voltage, i.e., 4.4 V and 4.6 V, are set to investigate the performance attenuation variability of different overcharge degrees. The intermittent overcharge cyclic aging condition is executed as follows: 1) 0.5 C constant current (CC) charge to 4.4 V/4.6 V; 2) Rest for 30 min; 3) 0.5 C CC discharge to 3.0 V; 4) Rest for 30 min; 5) 0.5 C constant current-constant voltage (CC-CV) charge to 4.2 V with current less than 0.05 C; 6) Rest for 30 min; 7) 0.2 C CC discharge to 3.0 V; 8) Rest for 30 min. In this way, it constitutes the typical intermittent overcharge cyclic aging conditions. For comparative investigation, another normal cyclic aging condition is set up, i.e., 0.5C CC-CV charge to 4.2 V with current less than 0.05 C and 0.5 C CC discharge to 3.0 V. The rest time is equally 30 min. All three conditions are performed 200 cycles.

2.3 Reference performance tests

In terms of capacity, the battery discharge capacity is continuously monitored during the cyclic aging process of the three operating conditions; in addition, the standard discharge capacity of the battery is also calibrated at intervals of 50 cycles using the standard charging and discharging profiles, and the number of cycles is three, with the discharge capacity of the last cycle being taken as the discharge capacity in this calibration process. The electrochemical impedance spectroscopy (EIS) tests are performed for every 50 cycles. The tested battery is charged to fully state of charge by using 0.5 C CC-CV charging profile. The battery impedance is measured by means of sinusoidal current excitation on the electrochemical workstation (Solartron Analytical 1470E, Fig. 1(c)). The current amplitude is 250 mA and the test frequency range is 10 kHz ~ 0.01 Hz. Before performing the next reference performance tests, the battery is discharged to the lower cut-off voltage of 3.0 V using a 0.2 C CC discharging file. Moreover, the incremental capacity-differential voltage analysis (IC-DV), a non-destructive analysis method, is used to analyze the degradation mechanism under two intermittent overcharge cyclic aging conditions and normal cyclic aging condition. The method of obtaining the IC-DV curves is by charging and discharging the battery using a low current rate, and 0.05 C is used in this study. The principle of the IC-DV method is to calculate the derivative of the capacity/voltage

with respect to the voltage/capacity. Similarly, the corresponding tests are performed every 50 cycles. The above reference performance tests are conducted at room temperature of about 25°C.

3 Results and discussion

3.1 Capacity retention analysis

As mentioned above, the intermittent overcharge frequency in this study is set at 0.5. Therefore, for the normal cyclic aging condition and the intermittent overcharge cyclic aging conditions, the voltage characteristics during their cycle tests are shown in Figs. 3(a), 3(c) and 3(e). An example of 10 cycles is shown in Figs. 3(b), 3(d) and 3(f), which shows the differences between the three cyclic aging conditions. The normal cyclic aging condition is completely in continuous operation within the defined normal voltage range, while the intermittent overcharge cyclic aging conditions are in abnormal continuous operation at different degrees beyond the normal upper cut-off voltage.

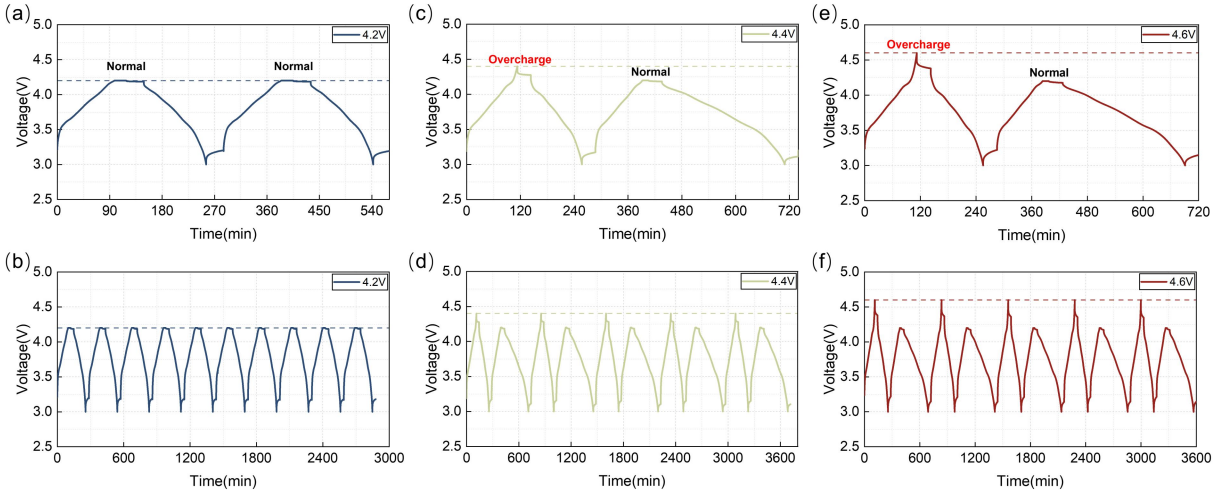

Figure 3: battery voltage characteristics. (a-b) normal cyclic aging condition; (c-d) intermittent overcharge cyclic aging condition at 4.4 V; (e-f) intermittent overcharge cyclic aging condition at 4.6 V.

Fig. 4 shows the evolution characteristics of the charge/discharge curves of the battery during cyclic aging under three operating conditions. Considering the basic characteristics of the intermittent overcharge cyclic aging conditions, the charge/discharge curves for 200 cycles are presented respectively based on parity. Obviously, the power and capacity of the battery decay in both the normal cyclic aging condition and the intermittent overcharge cyclic aging condition. Specifically, the shift of the charging and discharging curves in the intermittent overcharge cyclic aging condition is significantly greater than that in the normal cyclic aging condition, and the shift of the charging and discharging curves in the intermittent overcharge cyclic aging condition of 4.6 V is significantly greater than that in the intermittent overcharge cyclic aging condition of 4.4 V. The above shows that intermittent overcharge during long-term cyclic aging leads to accelerated degradation of battery power and capacity, and the degradation becomes more severe with the increase of the intermittent overcharge degree.

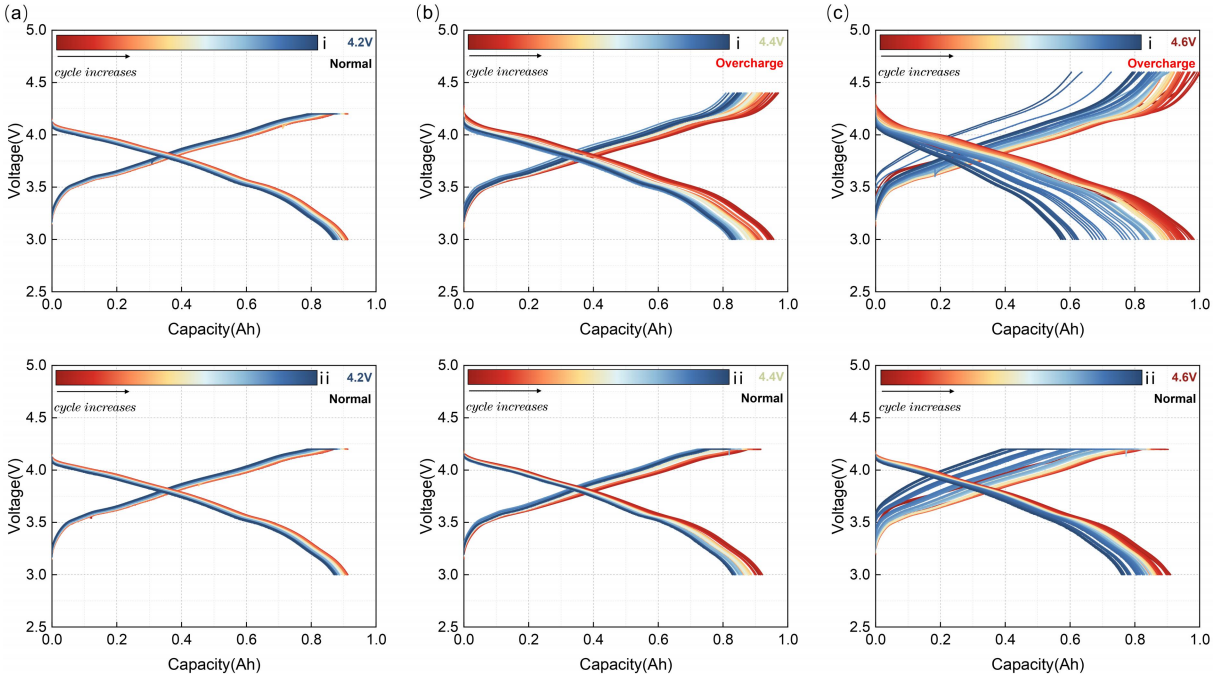

Figure 4: Evolution characteristics of the charge/discharge curves. (a) normal cyclic aging condition; (b) intermittent overcharge cyclic aging condition at 4.4 V; (c) intermittent overcharge cyclic aging condition at 4.6 V. (i) odd number of cycling; (ii) even number of cycling.

The discharge capacity attenuation trajectory under three cyclic aging conditions is shown in Fig. 5(a). The battery discharge capacity is calibrated with the same charging/discharging profile every 50 cycles, and the results are shown in Fig. 5(b). Overall, the discharge capacity of the normal cyclic aging condition is continuously higher than that of the intermittent overcharge cyclic aging condition. It is worth noting that the discharge capacity of the 4.4 V and 4.6 V intermittent overcharge cyclic aging conditions are comparable (the former is slightly higher than the latter) in the previous 150 cycles, while the two cyclic aging conditions begin to show a significant difference after 150 cycles, with the latter showing a nonlinear capacity degradation characteristic. After 200 cycles, the standard discharge capacity of the normal cyclic aging condition retains 96.8% of the initial capacity, while that of the two intermittent overcharge cyclic aging conditions retains 88.4% (4.4 V) and 80.2% (4.6 V) of the initial capacity.

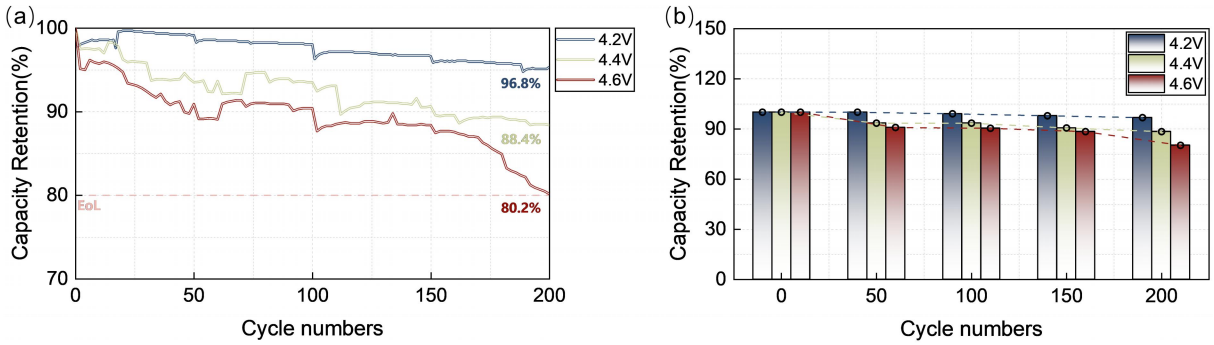

Figure 5: (a) discharge capacity attenuation trajectory under normal cyclic aging condition and two intermittent overcharge cyclic aging conditions; (b) battery state-of-health values at 50-cycle intervals.

3.2 EIS evolution analysis

The EIS results under three cyclic aging conditions are shown in Fig. 6. The results show that, except for the offset phenomenon in the direction of the horizontal axis, the overall shape of the impedance during the aging process shows obvious changes, mainly shown as a significant increase in the impedance arcs; comparing the three cyclic aging conditions with each other, the 4.6 V intermittent overcharge cyclic condition has the greatest growth, which indicates that the value of each impedance part under this condition also corresponds to the maximum increase.

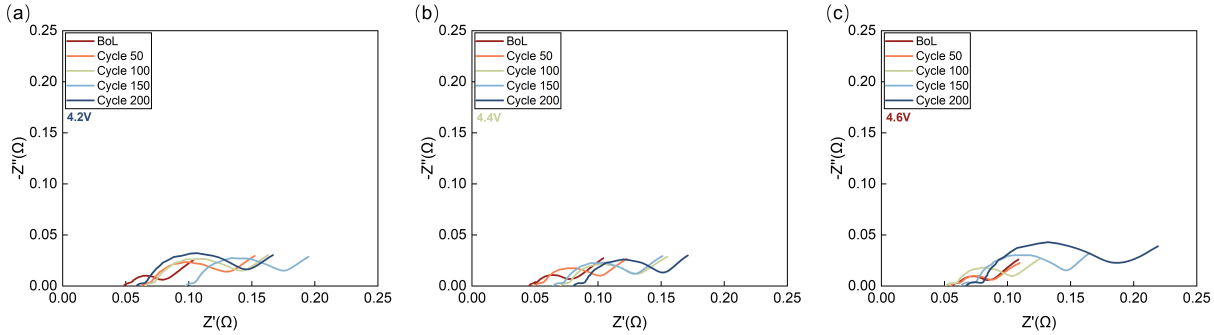

Figure 6: EIS results. (a) normal cyclic aging condition; (b) intermittent overcharge cyclic aging condition at 4.4 V; (c) intermittent overcharge cyclic aging condition at 4.6 V.

Due to the strong coupling characteristic of the different kinetic processes, it is necessary to specify the characteristics of the change in each impedance part in the case of an overall change in the EIS. Generally, the intersection of the EIS with the real axis of impedance corresponds to the ohmic resistance (R_{ohm}), the high-frequency part corresponds to the SEI process (R_{SEI}), the middle-frequency part corresponds to the charge transfer process (R_{ct}), and the low-frequency part corresponds to the solid-phase diffusion process (R_w) [9,10]. The quantification of the parameters corresponding to each kinetic process is realized through the fitting of the fractional order equivalent circuit model (ECM). Considering the overall characteristics of EIS, second-order ECM is used in this study. To achieve a good fitting, the capacitive C element in the R/C parallel connection link is substituted by the constant phase element (CPE). The EIS fitting results are shown in Fig. 7. It is shown that utilizing the second-order ECM enables experiment and fitting data to show good consistency in the high, middle, and low-frequency parts.

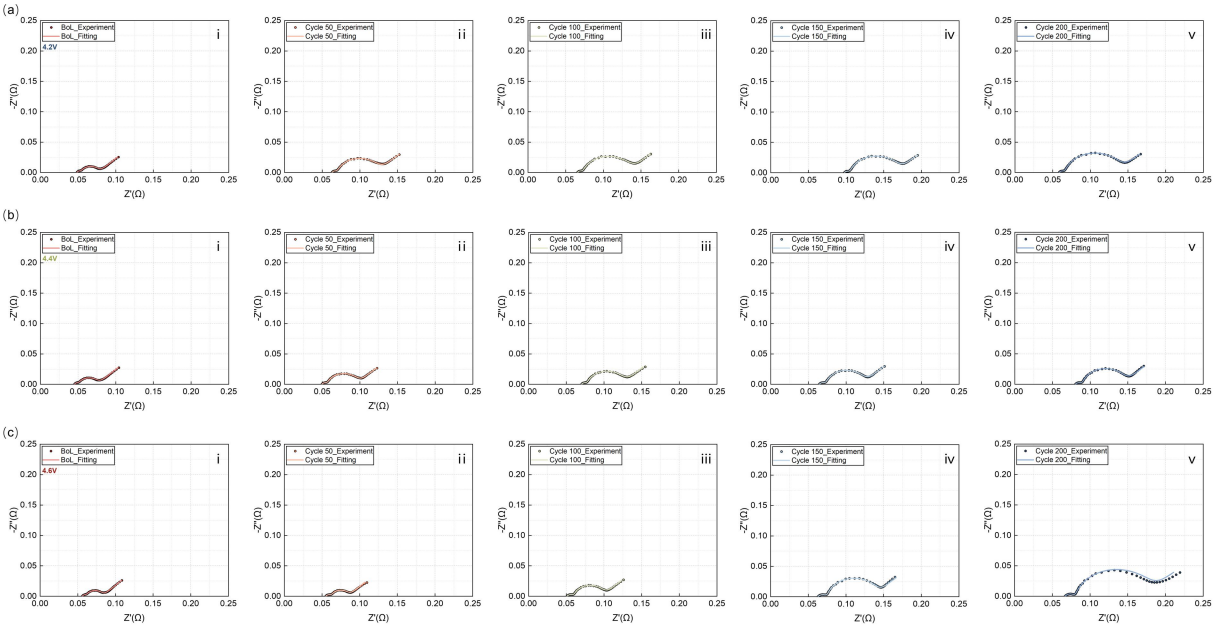

Figure 7: EIS fitting results. (a) normal cyclic aging condition; (b) intermittent overcharge cyclic aging condition at 4.4 V; (c) intermittent overcharge cyclic aging condition at 4.6 V. (i-v) BoL, Cycle 50, Cycle 100, Cycle 150 and Cycle 200.

The fitted values for each impedance part are shown in Fig. 8. Although R_{ohm} is a key parameter, its value, in addition to being related to the battery's state, would be affected by external factors such as external test fixtures and external equipment wiring, and therefore will not be analyzed accordingly here. It can be found that R_1 (R_{SEI}) and R_2 (R_{ct}) show an increasing trend under each cyclic aging condition. However, the growth patterns are not the same. In terms of R_1, the growth rate shows a pattern of 4.6 V > 4.4 V > 4.2 V. In terms of R_2, the normal cyclic aging condition and the 4.4 V intermittent overcharge cyclic aging condition show similar growth patterns (rapid in the early cycle and slowing down in the late cycle), while the 4.6 V intermittent overcharge cyclic aging condition shows an exponential increase after the 50th cycle and exceeds the above two cyclic aging conditions at the 150th cycle. The value change in the sum of R_1 and R_2 reflects the degree of the loss of lithium inventory (LLI), which is one of the important aging mechanisms, to some certain degree.

It can be found that, from the kinetic perspective, the degree of LLI for the 4.4 V intermittent overcharge cyclic aging condition and the normal cyclic aging condition are similar, while the LLI for the 4.6 V intermittent overcharge cyclic aging condition is significantly higher than both above conditions.

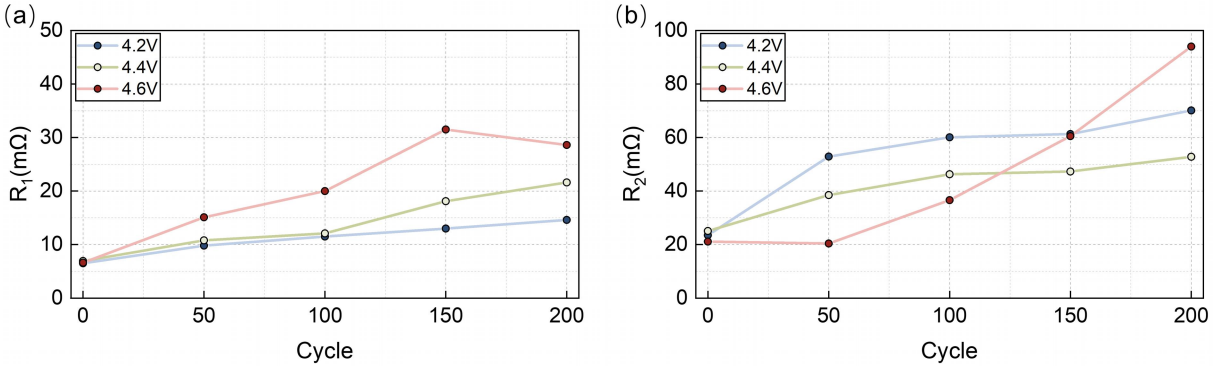

Figure 8: (a) R_1 values under different cycles; (b) R_2 values under different cycles.

Fitting EIS using ECM is an impedance analysis method that relies on a priori knowledge, whereas the distribution of relaxation times (DRT) analysis method can reveal more accurate information about the kinetic processes at different time scales without being influenced by a priori knowledge of the electrochemical device system [11,12]. In this study, the solution parameters involved in performing DRT calculations are set as follows: Gaussian for the discretization method, a combination of real and imaginary parts for the used data type, exclusion of inductive data, 2nd order for the regularization parameter, 0.0015 for the regularization parameter, 0.5 for the FWHM coefficient. The DRT analysis results of the EIS are shown in Fig. 9. According to the increasing order of relaxation time from left to right, the DRT characteristic peaks are attributed to R_{SEI} (peak ①), R_{ct} (peaks ②/③), and R_w (peak ④), respectively. Peak ④ exists with significant oscillatory characteristic, so the focus here is likewise on the mid- and high-frequency divisions of the DRT calculations. In terms of peak ①, the growth pattern follows the same order of 4.6 V > 4.4 V > 4.2 V. In terms of peak ②, all three cyclic aging conditions show a trend of significant increase of peak height and rightward offset of peak position, with the 4.6 V intermittent overcharge cyclic aging condition showing the largest change shown in these two aspects, especially after the 50th cycle. Moreover, for the 4.6 V intermittent overcharge cyclic aging condition, peak ③ disappears after the 150th cycle, leading to the peak merging characteristic. Overall, the DRT analysis results are consistent with the analysis conclusions obtained from the EIS fitting through the ECM.

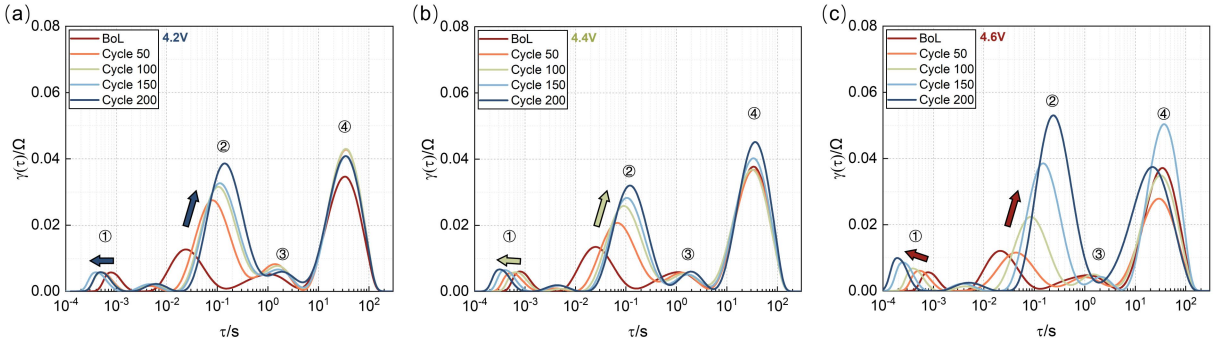

Figure 9: DRT curves. (a) normal cyclic aging condition; (b) intermittent overcharge cyclic aging condition at 4.4 V; (c) intermittent overcharge cyclic aging condition at 4.6 V.

3.3 IC-DV evolution analysis

As mentioned above, the charge/discharge rate for obtaining the IC-DV curves in this study is 0.05 C. However, even so, the obtained differential data still exhibits a large noise characteristic. Thus, in plotting the IC-DV curves, signal processing methods are used to reduce the noise effect on the analysis results. Specifically, the raw differential data are preprocessed using the adjacent average method [6]. It is done by adjusting the window size and comparing them with the original differential data to ensure that the peaks and valleys characteristics of the original differential data are still retained in the filtered smoothed data. The final window sizes are determined to be 3000 and 1500, respectively. The results are shown in Fig. 10. In addition to LLI, loss of active material (LAM) and conductivity loss (CL) are also important degradation modes. The

above three dominant aging mechanisms can be quantitatively compared by peak height change and peak position offset in the IC-DV curves. Specifically, the maximum voltage values in the IC curves are used to quantify CL, the peak height values associated with LAM in the IC curves are used to quantify LAM, and the maximum capacity values in the DV curves are used to quantify LLI [9]. First, it can be found that among the three conditions, CL changes significantly in the 4.6 V intermittent overcharge cyclic aging condition; however, its change is still minor compared to LAM and LLI. In terms of the change magnitude of LAM and LLI, the order of 4.6 V > 4.4 V > 4.2 V exhibits. Especially for the 4.6 V operating condition, the change in LAM and LLI after the 50th cycle is more pronounced. The above suggests that, from a thermodynamic perspective, intermittent overcharge cyclic aging condition at higher upper cut-off voltage causes more severe degradation of the active material and available lithium inventory inside the battery, which explains the nonlinear accelerated characteristic of its discharge capacity in the later stage.

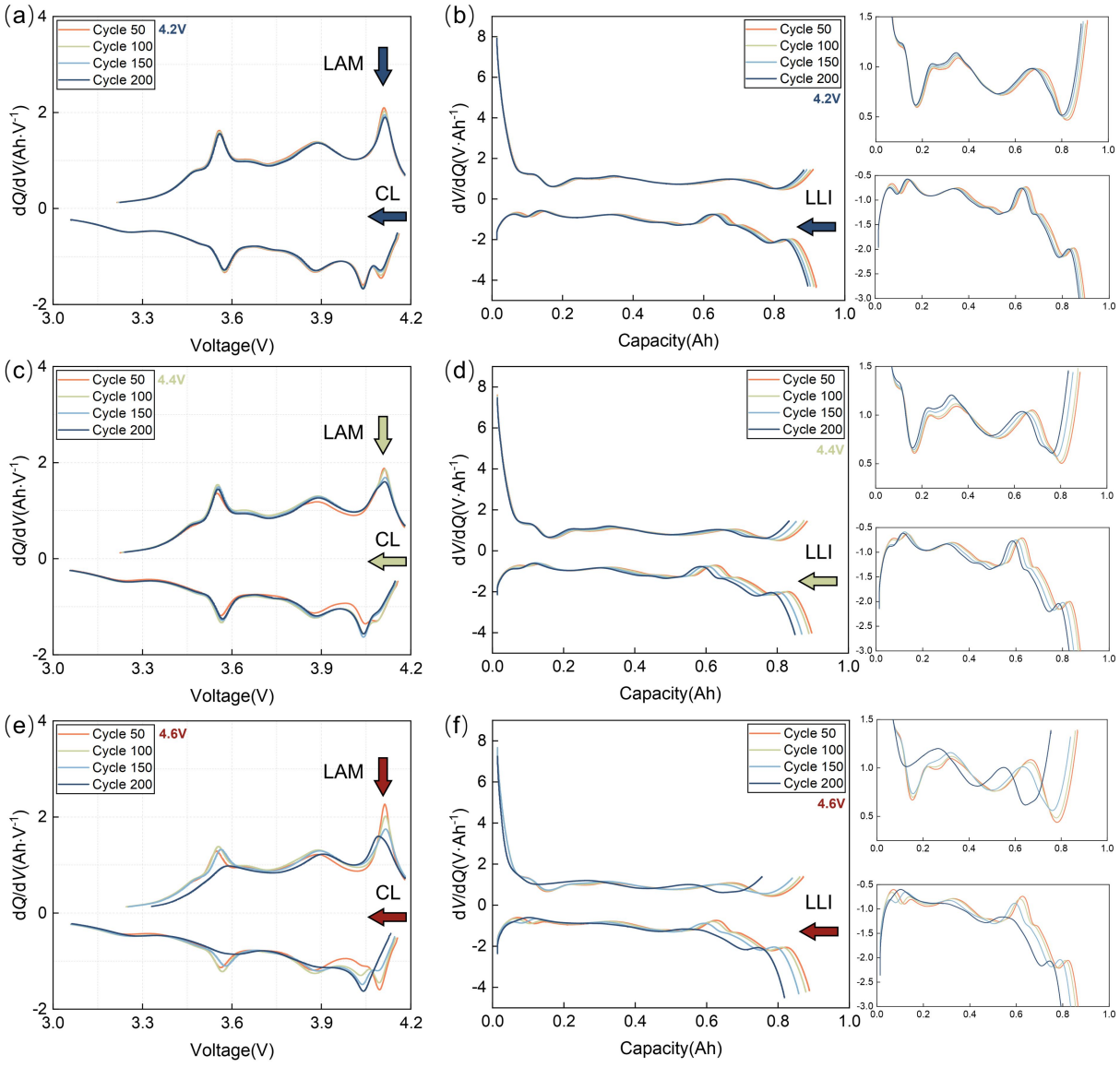

Figure 10: IC-DV curves. (a-b) normal cyclic aging condition; (c-d) intermittent overcharge cyclic aging condition at 4.4 V; (e-f) intermittent overcharge cyclic aging condition at 4.6 V.

4 Conclusions

In this study, the intermittent overcharge accumulation effect on electrochemical performance attenuation of silicon/graphite-based lithium-ion batteries is explored. The cyclic aging tests, including one type of normal cyclic aging condition (4.2 V as the upper cut-off voltage) and two types of intermittent overcharge cyclic aging conditions (4.4 V and 4.6 V as the upper cut-off voltage and 0.5 as the intermittent overcharge frequency), are carried out. The dominant aging mechanisms during battery cyclic aging are compared from both kinetic and thermodynamic perspectives by using two types of non-destructive analysis

methods, i.e., EIS and IC-DV. In the case of the EIS method, each impedance part is analyzed in detail by means of ECM and DRT. In the case of the IC-DV method, LAM and LLI are quantitatively compared by the change magnitude of the characteristic peak and maximum characteristic values. The results show that when the upper cut-off voltage increases (4.4 V), the accelerating capacity decay and impedance growth occur; after further increasing to a certain degree (4.6 V), it can cause the nonlinear decay of capacity and exponential growth of impedance (especially the charge transfer resistance R_{ct}), which is closely related to the more severe LAM and LLI under the 4.6 V intermittent overcharge cyclic aging condition. The findings of this study provide valuable theoretical support for the lifespan and safety control strategies of advanced lithium-ion battery material systems.

Acknowledgments

This work is financially supported by Shanghai Pilot Program for Basic Research and the National Natural Science Foundation of China (NSFC, Grant No. 52307248).

References

[1] Y. Wang et al., *Challenges and Opportunities to Mitigate the Catastrophic Thermal Runaway of High-Energy Batteries*, Advanced Energy Materials, ISSN 1614-6832, 13(2023), 2203841.

[2] K. Li et al., *Implementing expansion force-based early warning in $LiFePO_4$ batteries with various states of charge under thermal abuse scenarios*, Applied Energy, ISSN 0306-2619, 362(2024), 122998.

[3] N. Mao et al., *A systematic investigation of internal physical and chemical changes of lithium-ion batteries during overcharge*, Journal Power Sources, ISSN 0378-7753, 518(2022), 230767.

[4] Y. Zhang et al., *A multi-level early warning strategy for the LiFePO4 battery thermal runaway induced by overcharge*, Applied Energy, ISSN 0306-2619, 347(2023), 121375.

[5] G. Zhang et al., *Comprehensive Investigation of a Slight Overcharge on Degradation and Thermal Runaway Behavior of Lithium-Ion Batteries*, ACS Applied Materials & Interfaces, ISSN 1944-8244, 13(2021), 35054-35068.

[6] L. Zhang et al., *Degradation characteristics investigation for lithium-ion cells with NCA cathode during overcharging*, Applied Energy, ISSN 0306-2619, 327(2022), 120026.

[7] P. Huang et al., *Damage evolution mechanism and early warning using long short-term memory networks for battery slight overcharge cycles*, Renewable Energy, ISSN 0960-1481, 217(2023), 119171.

[8] J. Liu et al., *Quantitative analysis of aging and detection of commercial 18650 lithium-ion battery under slight overcharging cycling*, Journal of Cleaner Production, ISSN 0959-6526, 340(2022), 130756.

[9] R. Huang et al., *Revealing the low-temperature aging mechanisms of the whole life cycle for lithium-ion batteries (nickel-cobalt-aluminum vs. graphite)*, Journal of Energy Chemistry, ISSN 2095-4956, 106(2025), 31-43.

[10] W. Xu et al., *Investigation of lithium-ion battery degradation by corrected differential voltage analysis based on reference electrode*, Applied Energy, ISSN 0306-2619, 389(2025), 125735.

[11] Y. Zhou et al., *Estimation of overcharge-induced degradation state in lithium-ion cells using differential thermal voltammetry and distribution of relaxation times*, Journal of Energy Storage, ISSN 2352-152X, 97(2024), 112783.

[12] Z. Zhuang et al., *Distribution of relaxation times-based analysis of aging mechanisms and prediction of heating domain for alternating current pulse self-heating lithium-ion batteries*, Journal Power Sources, ISSN 0378-7753, 623(2024) 235442.

Presenter Biography

Gang Wei received the B.S. degree in automotive Engineering from Harbin Institute of Technology, Weihai, China, in 2020. He is currently working toward the Ph.D. degree in automotive engineering with the School of Automotive Studies, Tongji University, Shanghai, China. His research interests include battery degradation mechanism and battery thermal safety evaluation.